IOP Publishing New J. Phys. 26 (2024) 023060 https://doi.org/10.1088/1367-2630/ad2baf

New Journal of Physics
The open access journal at the forefront of physics

Deutsche Physikalische Gesellschaft DPG
IOP Institute of Physics

Published in partnership with: Deutsche Physikalische Gesellschaft and the Institute of Physics

OPEN ACCESS

RECEIVED
12 September 2023

REVISED
14 February 2024

ACCEPTED FOR PUBLICATION
21 February 2024

PUBLISHED
1 March 2024

Original Content from this work may be used under the terms of the Creative Commons Attribution 4.0 licence.

Any further distribution of this work must maintain attribution to the author(s) and the title of the work, journal citation and DOI.

PAPER

Energetics of magnetized Kerr-MOG and Kerr-Taub-NUT black holes within magnetic Penrose process

Husan Alibekov[1,4,*], **Ahmadjon Abdujabbarov**[1,2] **and Bobomurat Ahmedov**[1,2,3]

[1] Ulugh Beg Astronomical Institute, Astronomy St. 33, Tashkent 100052, Uzbekistan
[2] Institute of Theoretical Physics, National University of Uzbekistan, Tashkent 100174, Uzbekistan
[3] Institute of Fundamental and Applied Research, National Research University TIIAME, Kori Niyoziy 39, Tashkent 100000, Uzbekistan
[4] University of Tashkent for Applied Sciences, Str. Gavhar 1, Tashkent 100149, Uzbekistan
[*] Author to whom any correspondence should be addressed.

E-mail: alibekov@astrin.uz, ahmadjon@astrin.uz and ahmedov@astrin.uz

Keywords: magnetic field, magnetic Penrose process, Blandford–Znajek mechanism, gravitomagnetic charge, black hole energetics

Abstract

In this research paper, we have examined the impact of a gravitomagnetic charge on extracting energy from a rotating Kerr-Taub-NUT black hole and Kerr-MOG (MOdified Gravity known as Scalar-Tensor-Vector-Gravity (STVG)) black hole embedded in the magnetic field via the magnetic Penrose process (MPP). Our findings demonstrate that the gravitomagnetic monopole and MOG parameters both significantly influence the extraction of energy from a rotating black hole, exceeding the MPP for the Kerr black hole in terms of energy efficiency. After comparing the results of this study with the observational data, we were confident that our findings on the amplification of MPP by MOG and NUT parameters are nearly in line with the observations of ultrarelativistic particles in the cosmic rays.

1. Introduction

The Kerr spacetime is a vacuum solution to Einstein's field equation describing gravity around a rotating compact object that is both stationary and axisymmetric. It is described by two parameters: the total mass and spin of the collapsed object. Among various axisymmetric vacuum solutions, the Kerr geometry holds exceptional significance in the field of astrophysics. Recent observations conducted by the Event Horizon Telescope (EHT) [1] have successfully mapped the central compact radio source within the elliptical galaxy M87 [2] to a Kerr black hole, achieving an unprecedented level of angular resolution.

Nonetheless, alternative models to the Kerr black hole have not been conclusively dismissed, leading to suggestions to investigate whether the observed data aligns with other potential explanations for the central object in M87*. One proposal, for example, involves considering the potential existence of black holes with NUT (Newman-Unti-Tamburino) charges as an alternative to the Kerr black hole [3]. The goal of authors of [4] is to determine whether the presence of the NUT charge can be confirmed or ruled out in the central compact radio source of M87, an elliptical galaxy. To accomplish this, the observational parameters obtained from the initial image of M87*, made available by the EHT collaboration, are utilized. Additionally, a second vital aim of this study is to impose restrictions on the values of the spin parameter and the NUT parameter of M87* if a non-zero gravitomagnetic monopole does indeed exist [5]. By analyzing the data and observations, this investigation seeks to provide insights into the potential presence and characteristics of the NUT charge in M87*, while also evaluating the influence of the Kerr parameter [6].

If gravitomagnetic monopoles were to exist and exert an influence on the gravitational field, it could have significant implications for our understanding of spacetime. The Kerr-Taub-NUT spacetime represents a solution to Einstein's field equations describing a rotating black hole with a gravitomagnetic monopole charge. The presence of a gravitomagnetic monopole within the Kerr-Taub-NUT spacetime gives rise to several intriguing characteristics. Firstly, the spacetime no longer exhibits asymptotic flatness, indicating that it does not approach a flat spacetime at infinity [7–9]. This departure from asymptotic flatness has

© 2024 The Author(s). Published by IOP Publishing Ltd on behalf of the Institute of Physics and Deutsche Physikalische Gesellschaft

consequences for the behavior of particles and fields in the vicinity of the black hole. Another consequence is the emergence of closed timelike curves (CTCs). CTCs represent paths through spacetime that, if followed by an object, would enable it to travel back to its own past. In the context of the Kerr-Taub-NUT spacetime, the existence of gravitomagnetic monopoles can create regions where CTCs become possible.

Evidence supporting the existence of dark energy and dark matter in the Universe has been established through various observations, such as galactic rotation curves and the accelerated expansion of the Universe. These phenomena can be accounted for by introducing the cosmological constant Λ into the cosmological solutions of general relativity, along with hidden mass in the form of cold dark matter, constituting the standard ΛCDM cosmological model. Despite this, there are alternative theories that modify general relativity to explain these phenomena through intrinsic effects within extended gravity theories.

One such modification is known as Scalar-Tensor-Vector Gravity (STVG), also referred to as MOG (Modified Gravity), proposed by Moffat [10]. This theory has been applied to various astrophysical phenomena, including galaxy rotation curves [11, 12], black hole shadows [13, 14], and gravitational lensing [15–17]. Solutions for non-rotating and rotating black holes in MOG, identified as Schwarzschild-MOG and Kerr-MOG, respectively, have been derived in [18]. In order to prevent the breakdown of the MOG theory at short distances, a massive vector field has been incorporated into the theory, featuring a source charge denoted as $Q = \sqrt{\alpha G}M$. Here, G stands for the gravitational constant, M represents the mass of the central object, and α signifies the new coupling parameter. This inclusion introduces an extra repulsive force that gains prominence at the quantum level.

In the STVG theory, the vector field introduces an additional force beyond the scalar field, providing an extra contribution to the gravitational interaction. The vector field is associated with a preferred frame of reference and influences the behavior of gravity in a manner distinct from general relativity [10]. The inclusion of the vector field in STVG allows for modifications to gravitational phenomena beyond what can be explained by scalar-tensor theories alone. This additional degree of freedom can impact the dynamics of astrophysical systems, cosmological expansion, and other gravitational phenomena [19, 20]. The α parameter plays a crucial role in the STVG theory. It is a fundamental parameter that determines the strength of the additional gravitational forces introduced by the scalar and vector fields in STVG. The presence of a scalar field introduces a fifth force, which goes beyond the gravitational force described by general relativity. The magnitude of this additional force is determined by the α parameter [18]. A higher value of α corresponds to a more potent fifth force, whereas a lower value results in a weaker fifth force. Essentially, the α parameter governs the degree of interaction, or coupling strength, between the scalar field and matter.

Energy extraction from rotating black holes is a fascinating concept in theoretical astrophysics and has been the subject of various scientific studies and approaches. The energy extraction mechanisms (see for example [21–23] mainly revolve around exploiting the immense rotational energy of a rapidly spinning Kerr black hole. Two notable mechanisms for the energetics of black holes are the Penrose and Blandford–Znajek processes.

The Penrose process (PP) is a theoretical concept proposed by Roger Penrose in 1969 see, for details, [24]. It involves extracting energy from a rotating Kerr black hole by taking advantage of the ergosphere which is a region just outside the event horizon where the space-time is dragged along with the rotation of the Kerr black hole. In the Penrose process, a particle splits into two parts in the ergosphere of the black hole, with one part falling into the black hole and the other escaping to infinity. By carefully arranging the initial conditions of this process, the escaping part can gain more energy than the initial particle had. The energy gain of the escaping particle comes at the expense of the black hole's rotational energy, causing it to slow down its rotation. However, PP has some limitations, such as the difficulty of getting the extracted energy back to a useful form for practical applications due to the low cross section of the collision process [25].

The Blandford–Znajek process is another valuable theoretical mechanism for extracting energy from rotating black holes, proposed by Blandford and Znajek in 1977 [26]. This process operates on the principle of electromagnetic induction in the vicinity of the black hole. In the presence of a magnetic field that is anchored in the rotating black hole, the rotation of the black hole generates an electric potential difference across the magnetic field lines. As charged particles, such as ions or electrons, move along the magnetic field lines, they experience this electric potential difference, which can accelerate them to extremely high energies. Part of this energy can be extracted and utilized, similar to a generator in an electric power plant.

The Blandford–Znajek process is expected to be more efficient than the Penrose process for extracting energy from black holes, particularly for supermassive black holes found in the centers of galaxies. The powerful jets observed in active galactic nuclei (AGN) and quasars are believed to be the result of this process, where energy is extracted and funneled away in the form of relativistic jets of particles and radiation. During the three and half decades since its theoretical discovery, the Blandford–Znajek process of extracting

the rotational energy of black holes has become one of the foundations for explaining highly energetic phenomena in relativistic astrophysics.

It is important to underline that both the Penrose process and the Blandford–Znajek process are highly theoretical and have not been observed directly. The extreme conditions near rotating black holes make them difficult to study in detail, and their practical applications, if any, remain speculative. Nonetheless, exploring these mechanisms provides valuable insights into the behavior of black holes and the potential sources of energy in the Universe.

Since the original PP is not very efficient for its astrophysical applications for powering the central engine of highly energetic quasars and AGNs it was proposed in [27, 28] that in the presence of a test magnetic field in the hole vicinity of the magnetic Penrose process (MPP) occurs where the weak magnetic field could provide the energy required for a fragment to ride on negative energy orbit thereby overcoming the stringent velocity constraint of the original PP. In this sense, MPP is analogous to the Blandford–Znajeck (BZ) mechanism in which the rotational energy of the Kerr black hole is extracted through a purely electromagnetic process. Though both processes use the magnetic field as a catalyzation to extract rotational energy from the Kerr black hole, their kernel is quite different in spirit. For the former magnetic field provides the threshold energy for a particle to get into a negative energy orbit so that the other fragment goes out with enhanced energy while for the latter it generates an electric potential difference between the equatorial plane and the polar region, and it is the discharge of which that drives the energy flux out of the hole. In other words, MPP is still rooted in the spacetime geometry while BZ is essentially driven by electromagnetic interaction [29].

It was demonstrated that the MPP operates in three efficiency regimes, namely low, moderate, and ultra, depending on the magnetization and charging of spinning black holes in an astrophysical scenario. In ultra regime, MPP could power engines of such phenomena as ultra-high-energy cosmic rays, relativistic jets, fast radio bursts, quasars, AGNs, etc [21]. The distinguishing feature of the MPP is its super high efficiency exceeding 100 per cent (which was established in mid 1980 s for discrete particle accretion) of extraction of rotational energy of a rotating black hole electromagnetically for a magnetic field of milli Gauss order. Blandford–Znajek mechanism (BZ) could be treated as a high magnetic field limit MPP requiring a threshold magnetic field of order 10^4 G [30].

Motivated by our preceding studies [25, 31] on the analogue of gravitational synchrotron radiation by a massive particle rotating black hole in MOdified Gravity (MOG) known as Scalar-Tensor-Vector-Gravity (STVG) and classical Penrose process from Kerr-MOG and Kerr-Taub-NUT black holes we study here MPP on energy extraction from these black holes.

The paper is organized in the following way. In the next section 2 we study the dynamics of charged particles around the Kerr-Taub-NUT black hole in an asymptotically uniform magnetic field. Section 3 is devoted to the MPP of energy extraction from the Kerr-MOG and Kerr-Taub-NUT black holes. The last section 4 is devoted to the summary and discussion of the main results.

2. Dynamics of charged particles around the Kerr-Taub-NUT black hole in an asymptotically uniform magnetic field

The aim of this section is to examine the motion and dynamics of the charged particles orbiting around a Kerr-Taub-NUT black hole embedded in an asymptotically uniform Wald magnetic field.

2.1. Background spacetime

In the Boyer-Lindquist coordinates, the spacetime metric that characterizes the rotating Kerr-Taub-NUT black hole is presented as follows, see e.g. [32]

$$\begin{aligned} ds^2 = &-\frac{1}{\Sigma}\left(\Delta - a^2 sin^2\theta\right) dt^2 + \frac{\Sigma}{\Delta} dr^2 + \Sigma d\theta^2 + \frac{2}{\Sigma}\left[\Delta\chi - a\left(\Sigma + a\chi\right) sin^2\theta\right] dt d\phi \\ &+ \frac{1}{\Sigma}\left[\left(\Sigma + a\chi\right)^2 sin^2\theta - \chi^2\Delta\right] d\phi^2 , \end{aligned} \tag{1}$$

where the parameters Σ, Δ, and χ are determined by the definition of the aforementioned variables

$$\begin{aligned} \Sigma &= r^2 + (l + a\cos\theta)^2 , \\ \Delta &= r^2 - 2Mr - l^2 + a^2 , \\ \chi &= a\sin^2\theta - 2l\cos\theta . \end{aligned} \tag{2}$$

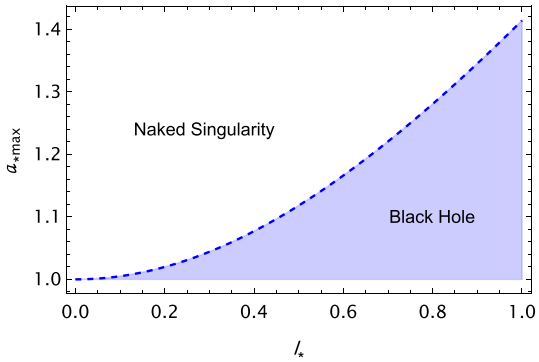

Figure 1. The relationship between the maximum spin of the black hole and the dimensionless gravitomagnetic charge l_* using the equation $a_{*\max} = \sqrt{1+l_*^2}$.

The quantities M, a, and l correspond to the total mass, the specific angular momentum of the black hole, and the gravitomagnetic NUT parameter of the central object, respectively. In [7] the Kerr-Taub-NUT metric has been described incorporating a non-zero constant denoted as c. This constant determines the position of the singularity. When c is equal to 1, the singularity is situated at $\theta = \pi$, while for $c = -1$, it is located at $\theta = 0$. For all other values of c, both singularities coexist. To establish symmetry between the north and south poles, the value of c is specifically chosen as 0. This decision is motivated by the observation that the Kerr-Taub-NUT metric demonstrates asymptotic flatness at spatial infinity [33], following the principles outlined by [34]. Therefore, by setting c equal to 0, we maintain the symmetrical relationship between the north and south poles in this particular case.

The equation $\Delta = 0$ determines the locations of the horizons, specifically at $r_\pm = M + \sqrt{M^2 + l^2 - a^2}$ and in most cases, $r_+ = r_h$ represents the outer horizon of the black hole, commonly referred to as the event horizon. The point at which the time-translation Killing vector $\xi(t) = \frac{\partial}{\partial t}$ becomes null is known as the static limit. The characteristics of the black hole's ergosphere can be explained as follows [25, 35]

$$r_e = M + \sqrt{M^2 + l^2 - a^2\cos^2\theta}\,. \tag{3}$$

The equations provided above reveal that at the poles ($\theta = 0$ or π), the radius of the ergoregion aligns with the event horizon. However, on the equatorial plane ($\theta = \pi/2$), the ergoregion's radius is affected by both the NUT parameter and the mass, resulting in $r_e = M + \sqrt{M^2 + l^2}$. In contrast, within the Kerr spacetime, the ergoregion radius at $\theta = \pi/2$ is given by $r_e = 2M$. By setting the denominator of the metric component g_{tt} to zero, we can deduce the following expression [4]

$$r = 0\,, \qquad \theta = \cos^{-1}(-l/a)\,. \tag{4}$$

In the Kerr-Taub-NUT spacetime, the singularity is located at this point [4, 35]. It is important to note that spacetime becomes free from singularities when $l > a$, indicating the presence of a regular black hole. On the other hand, for $l \leqslant a$, the Kerr-Taub-NUT spacetime describes a black hole with $|a| \leqslant \sqrt{M^2 + l^2}$ and a naked singularity when $|a| > \sqrt{M^2 + l^2}$. For simplicity, we will frequently utilize the dimensionless parameters $a_* = a/M$ and $l_* = l/M$. In theory, for a Kerr-Taub-NUT black hole, the values of a_* and l_* can be arbitrarily large (subject to the condition $|a_*| \leqslant \sqrt{1+l_*^2}$). However, in this study, we assume that the gravitomagnetic charge values are constrained to $l_* \leqslant 1$ for selected black hole candidates. This restriction also limits the range of the black hole's spin to $|a_*| \leqslant 2$. Figure 1 illustrates the correlation between the maximum spin of the black hole and the dimensionless gravitomagnetic charge l_*. It is commonly understood that a Kerr black hole has a maximum spin of $a_{*\max} = 1$, but in the presence of a gravitomagnetic charge, this maximum spin increases to $a_{*\max} = \sqrt{1+l_*^2}$.

2.2. Circular orbits

In this section, we are specifically studying the motion of a charged particle. The particle has a mass of m and an electric charge of q. This motion takes place in the presence of a Kerr-Taub-NUT gravitational field, which possesses axial symmetry. Moreover, there is a magnetic field surrounding the black hole, which is distributed uniformly and aligned parallel to the black hole's axis of rotation. The behavior of charged particles interacting with magnetic fields remains fundamentally unchanged despite the curvature of

spacetime. The gravitational field in curved spacetime alters the trajectory of a charged particle, causing deviations from a straight path.

A Killing vector is a vector field on a manifold that generates an isometry, representing a symmetry of the spacetime. It captures the conserved quantities associated with the symmetries of the spacetime [36]. In this spacetime, we will take advantage of the presence of a timelike Killing vector $\xi^{\mu}_{(t)}$ and a spacelike Killing vector $\xi^{\mu}_{(\phi)}$. These vectors play a crucial role in maintaining the stationarity and axial symmetry of the geometry, satisfying the Killing equations [37, 38]

$$\nabla_{\mu}\xi_{\nu} + \nabla_{\nu}\xi_{\mu} = 0\,, \tag{5}$$

where ξ_{μ} represents the components of the Killing vector and ∇_{μ} denotes the covariant derivative. The conserved quantities associated with Killing vectors are derived by applying Killing's equation to the equations of motion of particles or fields in the spacetime. The presence of stationarity and axial symmetry in the Kerr-Taub-NUT black hole spacetime allows for the selection of the vector potential for the weak magnetic field, as discussed in. This vector potential, which satisfies the vacuum Maxwell equations with a Lorentz gauge condition ($A^{\alpha}_{;\alpha} = 0$), can be represented as a linear combination of the spacetime Killing vectors [38]

$$A^{\mu} = C_1\xi^{\mu}_{(t)} + C_2\xi^{\mu}_{(\phi)}\,. \tag{6}$$

Due to the weak nature of the magnetic field, which can be characterized as a test field, we have the liberty to freely select the magnetic field configuration. Additionally, the parameters C_1 and C_2 can be readily derived by considering the asymptotic properties and ensuring the electrical neutrality of the source (appendix B), as well as the uniformity of the external magnetic field [39]

$$C_1 = aB\,, \quad C_2 = \frac{B}{2}\,. \tag{7}$$

Consequently, the non-zero components of the four-vector potential for the asymptotically uniform magnetic field can be expressed as follows [21]

$$A_t = \frac{\mathcal{B}}{2}\left(g_{t\phi} + 2ag_{tt}\right)\,, \quad A_{\phi} = \frac{\mathcal{B}}{2}\left(g_{\phi\phi} + 2ag_{t\phi}\right)\,. \tag{8}$$

The presence of the rotation parameter 'a' leads to terms that contribute to the Faraday induction, thereby generating an electric potential and producing an induced electric field [38]. The resulting potential difference between the black hole horizon and infinity can be described as [39, 40]

$$\Delta\phi = \phi_H - \phi_{\infty} = \frac{Q - 2aMB + 2lMB}{2M}\,. \tag{9}$$

As a result, charged particles are selectively accreted into the rotating black hole. This process resembles the phenomenon observed in the presence of a rotating conductor immersed in a magnetic field. Therefore, it is necessary to rephrase the expressions (8) that represent the non-zero covariant components of the four-vector potential [41–43]

$$\begin{aligned} A_t &= \frac{\mathcal{B}}{2}\left(g_{t\phi} + 2ag_{tt}\right) - \frac{Q}{2M}g_{tt} - \frac{Q}{2M}\,,\\ A_{\phi} &= \frac{\mathcal{B}}{2}\left(g_{\phi\phi} + 2ag_{t\phi}\right) - \frac{Q}{2M}g_{t\phi}\,. \end{aligned} \tag{10}$$

In the context of Kerr-Taub-NUT spacetime, the maximum value of the induced black hole charge, denoted as Q ([39]), corresponds to $2(a-l)\mathcal{B}M$ when accounting for the influence of the induced electric charge Q on the black hole. Consequently, the electromagnetic potential is reduced compared to the Wald charge

$$A_t = \frac{\mathcal{B}}{2}\left(g_{t\phi} + 2lg_{tt} - 2\left(a-l\right)\right)\,, \quad A_{\phi} = \frac{\mathcal{B}}{2}\left(g_{\phi\phi} + 2lg_{t\phi}\right)\,. \tag{11}$$

It is crucial that, even under these restrictive circumstances, the A_t component remains nonzero, leading to a potentially powerful acceleration effect near massive black holes situated within intense magnetic fields ([23]).

If we disregard the effects of radiation-reaction force, we can determine the equation of motion governing a massive particle as follows [21, 30]

$$\frac{Du^{\mu}}{d\tau} = \frac{q}{m} F^{\mu}_{\ \nu} u^{\nu} \,. \tag{12}$$

An alternate way to express this is

$$\ddot{x}^{\mu} + \Gamma^{\mu}_{\nu\lambda} \dot{x}^{\nu} \dot{x}^{\lambda} = \frac{q}{m} F^{\mu}_{\ \nu} \dot{x}^{\nu} \,, \tag{13}$$

resulting from the Lagrangian given by

$$\mathcal{L} = \frac{1}{2} g_{\mu\nu} \dot{x}^{\mu} \dot{x}^{\nu} + \frac{q}{m} A_{\mu} \dot{x}^{\mu} \,. \tag{14}$$

The given expressions pertain to a test particle, with m representing its mass and $\dot{x}^{\mu}$ denoting its four-velocity. An anti-symmetric tensor is defined as $F_{\mu\nu} = \partial_{\mu} A_{\nu} - \partial_{\nu} A_{\mu}$.

The conservation of the generalized four-momentum $P_{\mu} = m u_{\mu} + q A_{\mu}$ implies that its two components, which correspond to the energy and angular momentum of the particle, are preserved. These components can be linked to the Killing vectors in a particular manner

$$\begin{aligned} \xi^{\mu}_{(t)} \frac{P_{\mu}}{m} &= g_{tt} \frac{dt}{d\tau} + g_{t\phi} \frac{d\phi}{d\tau} + \frac{q}{m} A_t = -\mathcal{E} \,, \\ \xi^{\mu}_{(\phi)} \frac{P_{\mu}}{m} &= g_{\phi\phi} \frac{d\phi}{d\tau} + g_{t\phi} \frac{dt}{d\tau} + \frac{q}{m} A_{\phi} = \mathcal{L}_a \,, \end{aligned} \tag{15}$$

where $\mathcal{E} = E/m$ and $\mathcal{L}_a = L/m$.

The equation for Hamilton–Jacobi of a particle with mass m can be expressed as [44]

$$g^{\mu\nu} \left(\frac{\partial \mathcal{S}}{\partial x^{\mu}} - q A_{\mu} \right) \left(\frac{\partial \mathcal{S}}{\partial x^{\nu}} - q A_{\nu} \right) = -m^2 \,. \tag{16}$$

The solution to the above equation is related to the energy, E, and angular momentum, L, of the test particle. It can be decomposed as $\mathcal{S} = -Et + L\phi + \mathcal{S}_r + \mathcal{S}_{\theta}$. By substituting this solution into equation (A.6), one obtains

$$g^{rr} \left(\frac{\partial \mathcal{S}_r}{\partial r} \right)^2 + g^{\theta\theta} \left(\frac{\partial \mathcal{S}_{\theta}}{\partial \theta} \right)^2 + g^{tt} \left(E + q A_t \right)^2 - 2 g^{t\phi} \left(E + q A_t \right) \left(L - q A_{\phi} \right) + g^{\phi\phi} \left(L - q A_{\phi} \right)^2 = -m^2 \,. \tag{17}$$

By performing certain basic algebraic calculations, we get the ensuing expression

$$\left(\mathcal{E} + \frac{q}{m} A_t \right)^2 - 2\omega \left(\mathcal{E} + \frac{q}{m} A_t \right) \left(\mathcal{L}_a - \frac{q}{m} A_{\phi} \right) + \frac{g_{tt}}{g_{\phi\phi}} \left(\mathcal{L}_a - \frac{q}{m} A_{\phi} \right)^2 + \left(g_{rr} \dot{r}^2 + g_{\theta\theta} \dot{\theta}^2 + 1 \right) \psi = 0 \,. \tag{18}$$

To put it differently, $\mathcal{S}_{\theta}$ and $\mathcal{S}_r$ represent functions that depend on θ and r, respectively, and the conditions are satisfied when $\omega = -g_{t\phi}/g_{\phi\phi}$ is greater than zero and $\psi = g_{tt} - g^2_{t\phi}/g_{\phi\phi}$ is less than zero.

Based on the given conditions of a massive particle in a circular orbit with zero radial velocity and zero angular velocity, it can be observed that the motion of the particle is confined within a certain range. This can be further understood by studying the effective potential as described in [21, 45]

$$V_{\rm eff} = -\frac{q}{m} A_t + \omega \left(\mathcal{L}_a - \frac{q}{m} A_{\phi} \right) + \left[(-\psi) \left(\frac{\left(\mathcal{L}_a - \frac{q}{m} A_{\phi} \right)^2}{g_{\phi\phi}} + 1 \right) \right]^{\frac{1}{2}} . \tag{19}$$

Meeting the requirement of $V_{\rm eff} = E$, which is a widely recognized method for comprehending the behavior of test particles in the vicinity of black holes, can be achieved through effective potential. The effective potential plays a critical role in determining the allowed orbits around a black hole, making it of utmost importance. By examining the shape of the effective potential, we can acquire a comprehensive understanding of the particle's motion characteristics and the stability of its orbits. In most cases, circular orbits manifest at the minima of the effective potential. The radius of a circular orbit is determined by the exact position of the

minimum within the effective potential. By determining the minimum value of the effective potential, we can establish the position of the innermost stable circular orbit (ISCO). The ISCO is the smallest possible path where a massive particle can maintain a stable circular trajectory without being drawn into the black hole or ejected into space. To simplify the analysis, we can focus on the movement of a massive particle in the equatorial plane, which means the effective potential only depends on the radial coordinate, denoted as $V_{\rm eff}(r)$. Using the conventional approach, we can find the position of the ISCO by meeting the following criteria: the effective potential is equal to the particle's energy ($V_{\rm eff}(r) = E$), the derivative of the effective potential for r is zero ($V'_{\rm eff}(r) = 0$), and the second derivative of the effective potential concerning r is less than or equal to zero ($V''_{\rm eff}(r) \leqslant 0$). It is worth noting, however, that computing equation (19) analytically is extremely challenging. Nevertheless, it is crucial to emphasize the significance of the ISCO in astrophysical observations, as it can greatly impact the emission of radiation and the behavior of matter that enters the black hole. Furthermore, studying the ISCO can provide valuable insights into the characteristics of black holes and serve as a platform for investigating both general relativity and alternative theories of gravity.

To provide a more straightforward explanation, the behavior of particles near the Kerr-MOG spacetime with a magnetic field is described in appendix A.

3. Magnetic Penrose process

Now, let us consider a situation where particle 1, which could possess a charge, undergoes decay near the horizon in the equatorial plane, resulting in the formation of two charged fragments 2 and 3. By adhering to the principles of energy and angular momentum conservation after the decay process, we can represent this phenomenon in the following manner

$$E_1 = E_2 + E_3\ , \quad m_1\dot{r}_1 = m_2\dot{r}_2 + m_3\dot{r}_3\ , \tag{20}$$

$$L_1 = L_2 + L_3\ , \quad 0 = m_2\dot{\theta}_2 + m_3\dot{\theta}_3\ , \tag{21}$$

$$q_1 = q_2 + q_3\ . \tag{22}$$

If the dot represents differentiation to the proper time of the particle, and particle 2 has negative energy compared to infinity, then particle 3 obtains energy $E_2 = E_1 - E_2$ that is greater than the energy of incident particle 1. The absorption of negative energy into the black hole leads to an extraction of its rotational energy. Now, we once again analyze the circular motion of a massive particle, which has a four-velocity denoted as $\dot{x}^\mu = \dot{t}(1, v, 0, \Omega)$, where $v = dr/dt$ and $\Omega = d\phi/dt$. By making use of the normalization of the four-velocity, [31, 45] calculate the angular velocity of particle 1 as

$$\Omega_1 = \frac{-\left(u_t^2 + g_{tt}\right) g_{t\phi} + u_t\sqrt{(-\psi)\left(u_t^2 + g_{tt}\right) g_{\phi\phi}}}{u_t^2 g_{\phi\phi} + g_{t\phi}^2}\ . \tag{23}$$

In this context, the quantity $u_t = -(E_1 + q_1\Phi_t)/m_1$, represents a specific parameter. Moreover, the angular velocity of the divided fragments is denoted as $\Omega_2 = \Omega_+$ and $\Omega_3 = \Omega_-$, where the symbols $\Omega_\pm$ are defined as [46]

$$\Omega_\pm = -\frac{g_{t\phi}}{g_{\phi\phi}} \pm \sqrt{-\frac{\psi}{g_{\phi\phi}}}\ . \tag{24}$$

By applying the principles of conservation laws, it is possible to demonstrate that the angular velocities of particles at the splitting point obey a certain relationship

$$m_1 u_1^\phi = m_2 u_2^\phi + m_3 u_3^\phi\ . \tag{25}$$

Using equation (15), we obtain the following expression

$$u_i^\phi = -\left(\mathcal{E}_i + \frac{q_i}{m_i} A_t\right)\frac{\Omega_i}{X_i}\ , \tag{26}$$

where $\mathcal{E}_i = E_i/m_i$ and $X_i = g_{tt} + \Omega_i g_{t\phi}$. As a consequently, equation (25) can be expressed as

$$m_1\left(\mathcal{E}_1+\frac{q_1}{m_1}A_t\right)\frac{\Omega_1}{X_1}=m_2\left(\mathcal{E}_2+\frac{q_2}{m_2}A_t\right)\frac{\Omega_2}{X_2}+\ m_3\left(\mathcal{E}_3+\frac{q_3}{m_3}A_t\right)\frac{\Omega_3}{X_3}\ . \tag{27}$$

Following various algebraic manipulations, the energy of the particle that escapes can be obtained in the following representation

$$E_3=\Xi\left(E_1+q_1A_t\right)-q_3A_t\ , \tag{28}$$

where

$$\Xi=\frac{\Omega_1-\Omega_2}{\Omega_3-\Omega_2}\frac{X_3}{X_1}\ ,\quad X_i=g_{tt}+\Omega_i g_{t\phi}\ . \tag{29}$$

The efficiency of the MPP can be defined by the equation $\eta_{\rm MPP}=E_3/E_1-1$, where E_3 represents the energy of the outgoing particle and E_1 represents the energy of the incident particle. Using equation (28), we can write the energy efficiency of the MPP as

$$\eta_{\rm MPP}=\Xi-1+\left(q_1\Xi-q_3\right)\frac{A_t}{E_1}\ . \tag{30}$$

Plugging in the expressions for $(\Omega_1,\Omega_2,\Omega_2)$ and (X_1,X_3) into equation (29), we obtain the following result

$$\Xi=\frac{1}{2}\left(1+\sqrt{1+\frac{g_{tt}}{u_t^2}}\right)\ , \tag{31}$$

where, it is important to note that the velocity component u_t is connected to the energy E through the expression $mu_t=-\left(E+qA_t\right)$, and performing some fundamental algebraic operations, we can express the energy efficiency for the MPP as follows

$$\eta_{\rm MPP}=\frac{1}{2}\left(\sqrt{1+\frac{g_{tt}}{u_t^2}}-1\right)\left(1+\frac{q_1}{E_1}A_t\right)+\frac{q_1-q_3}{E_1}A_t\ . \tag{32}$$

3.1. A comparison between Kerr-MOG and Kerr-Taub-NUT for two different energy extraction models

We also know that there is another type of energy extraction model, well-known as the Blandford–Znajek mechanism [26]. However, the MPP and the Blandford–Znajek mechanism are different mechanisms for extracting energy from a rotating black hole. The MPP involves the interaction between the black hole's magnetic field and the plasma around it ([30]). In contrast, the Blandford–Znajek mechanism involves the extraction of energy from the black hole's spinning magnetic field. Both mechanisms are related to the black hole's rotation and magnetic field, but they operate in different ways and have different efficiencies [47].

Even though these ideas exist, it is feasible to compare these two energy extraction models with each other under certain conditions. We will attempt to complete this task in the following subsubsection.

3.1.1. Classification of magnetic Penrose process

The efficiency of the MPP in extracting energy from a black hole varies depending on the strength of the magnetic field and can be classified into three regimes with different levels of energy efficiency. These regimes range from low to moderate to ultra-high.

If there is no magnetic field present, the MPP reverts back to the ordinary Penrose process, which has a lower limit for maximum efficiency. So, this is called the low regime of the MPP, and it can be expressed as

$$\eta_{\rm MPP}^{\rm low}=\eta_{\rm PP}^{\rm (Kerr-Taub-NUT)}=\frac{1}{2}\left(\sqrt{1+g_{tt}}-1\right)\ . \tag{33}$$

The absence of a magnetic field is depicted in figure 2, and it illustrates that the maximum efficiency of energy extraction from the Kerr-Taub-NUT black hole can reach approximately $\sim 036\%$ for a specific value of the dimensionless gravitomagnetic charge. By contrast, if the gravitomagnetic charge of a black hole is absent, then we can return to the original Penrose process, $\eta_{\rm MPP}^{\rm low}=\eta_{\rm PP}^{\rm (Kerr)}=\left(\sqrt{2}-1\right)/2\approx 0.207$ or 20.7% [24, 45]. This value corresponds to the Kerr black hole that is extremely rotating.

If each particle is charged ($q_1\neq 0$), the efficiency can be computed using equation (32) in its entirety. However, in the presence of magnetic fields affecting elementary particles, electromagnetic forces take

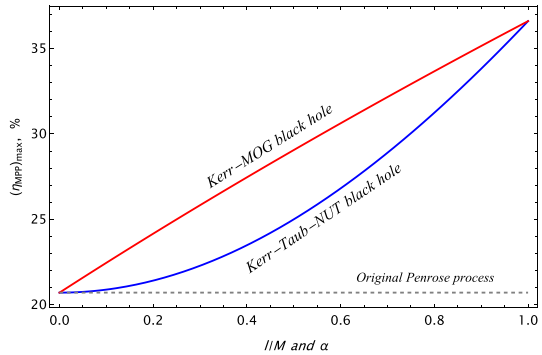

Figure 2. In the absence of a magnetic field, the extent to which a black hole can achieve its maximum energy efficiency is dictated by how it relates to the dimensionless gravitomagnetic charge l/M (represented by the blue solid line) and the STVG parameter α (represented by the red solid line).

precedence within the system, indicating that $\left|\frac{q}{m}A_t\right| \gg \left|mu_t\right|$. By linking this observation to equation (32), it becomes feasible to streamline the expression into the following form

$$\eta_{\rm MPP}^{\rm mod} \approx \frac{q_3}{q_1} - 1 + \eta_{\rm MPP}^{\rm low} \approx \frac{q_3}{q_1} + \frac{1}{2}\left(\sqrt{1+g_{tt}} - 3\right) . \tag{34}$$

The moderate regime of the MPP is in operation when q_3 is greater than q_1, effectively counteracting the gravitational electric field produced by a black hole. If we consider two particles with charges q_3 and q_1, respectively, and the ratio q_3/q_1 is an integer, it aligns with the principle of charge quantization. From a theoretical standpoint, in the vicinity of a black hole undergoing the MPP, the presence of multiple protons can result in various interactions, including proton-proton scattering and particle-antiparticle annihilation. These interactions can lead to the generation of secondary particles or the alteration of the initial proton trajectories. Secondary particles produced in these interactions, such as proton-proton scattering or particle-antiparticle annihilation, typically possess charge values that are integer multiples of the elementary charge. Consequently, their charges can be positive, negative, or zero, contingent upon the specific particles involved and the conservation of charge in the given interaction. For instance, in proton–proton scattering, the resulting secondary particles may include positively charged particles like protons or positively charged pions (π^+), as well as negatively charged particles like negatively charged pions (π^-) or antiprotons. All these charges correspond to integer multiples of the elementary charge.

This moderate regime of the MPP bears a direct resemblance to the well-known Blandford–Znajek mechanism. In both instances, the driving force is a quadrupole electric field resulting from the twisting of magnetic field lines caused by the black hole's frame-dragging effect [26]. It is crucial to mention that the efficiency of both the Blandford–Znajek mechanism and the moderate regime of the MPP cannot achieve excessively high levels due to inherent limitations imposed by the surrounding plasma's overall neutrality near the black hole. In the moderate regime of the MPP, it closely approximates the Blandford–Znajek mechanism, which clarifies why numerical simulations of the process do not display exceptionally high efficiency [47, 48].

The MPP has the potential for a third stage that is extremely efficient and deserves close investigation, leading to important predictions [23]. When particle 1 has no charge ($q_1 = 0$) and an energy of $E_1 = m_1$, then splits into two fragments with electrical charges, it becomes apparent that the efficiency equation (32) can be simplified as

$$\eta_{\rm MPP}^{\rm ultra} = \eta_{\rm MPP}^{\rm low} - \frac{q_3}{m_1}A_t = \frac{1}{2}\left(\sqrt{1+g_{tt}} - 1\right) - \frac{q_3}{m_1}A_t . \tag{35}$$

The efficiency of the mechanical Penrose process, indicated by $\eta_{\rm MPP}^{\rm low}$ in equation (35), depends entirely on geometric factors. In the absence of a gravitomagnetic charge, its value varies from 0 when $a = 0$ to 0.207 when $a = 1$. Additionally, when the spin and magnetic field are aligned ($a\mathcal{B} > 0$), it is evident that the A_t component of the vector potential assumes negative values above the horizon. For elementary particles like electrons and protons, which typically have high charge-to-mass ratios (q/m), the term $-q_3A_t/m_1$ has the most significant impact on equation (35). Consequently, in this specific scenario, the expression for efficiency can be reformulated as follows

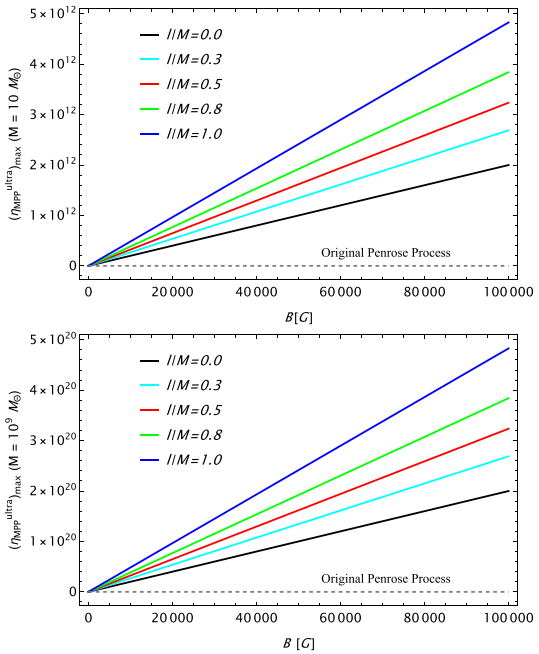

Figure 3. Efficiency in the ultra-high regime of the MPP is observed for two types of black holes: (above) a black hole with a stellar mass of 10 times the solar mass; and (bottom) a supermassive black hole weighing 10^9 times the solar mass. The efficiency is evaluated with respect to the original Penrose process for a black hole with an extremal spin, indicated by the dashed horizontal line. The colored curves represent different gravitomagnetic charges.

$$\eta_{MPP}^{ultra} \approx -\frac{q_3}{m_1} A_t \,. \tag{36}$$

If the alignment between spin and magnetic field exists, the escaping particles must have charges in opposite directions ($a\mathcal{B} < 0$), which can be significantly large for elementary particles. In this case, q_3 must be negative to achieve positive energy efficiency. Consequently, the MPP enters a state of ultra-high efficiency, resulting in the transfer of exceptionally high energy to the escaping particle. Figure 3 illustrates the assessment of the MPP's effectiveness in the ultra-high regime for two categories of black holes: a stellar mass black hole weighing ten times that of the Sun and a supermassive black hole weighing 10^9 times that of the Sun. The efficiency evaluation is based on a comparison with the original Penrose process for a black hole with maximum spin, indicated by the dashed horizontal line. The various gravitomagnetic charges are represented by the colored curves. The results we have obtained align with the observations made. The following section will demonstrate how our findings correspond with the observed words.

By using the MPP on the beta-decay of a neutron in the presence of a standard supermassive black hole (SMBH) with a mass of $10^9 M_\odot$ and a magnetic field strength of 10^4 G, it is possible to observe the release of a proton from the extremely rotating black hole (Kerr-Taub-NUT) with a certain amount of energy

$$E_{p+} = \mathcal{L}^* \left(\frac{q}{e}\right) \left(\frac{m}{m_{p+}}\right)^{-1} \left(\frac{\mathcal{B}}{10^4 G}\right) \left(\frac{M}{10^9 M_\odot}\right) eV \,, \tag{37}$$

where $\mathcal{L}^* = 1.62 \times 10^{20}(l + \sqrt{1 + l_*^2})$ and, l_*—the dimensionless NUT parameter. Figure 4 presents the correlation between proton energy and the magnetic field for different black hole masses and, in figure 5, it has been illustrated that the relationship between proton energy and magnetic field for different values of gravitomagnetic charge.

The MPP and the Blandford–Znajek mechanism share commonalities, but they differ in terms of the physical processes involved and the areas in which they are applied. The MPP operates by causing particle splitting near the event horizon, whereas the Blandford–Znajek mechanism relies on interactions with magnetic fields. The MPP has primarily been studied in relation to phenomena like gamma-ray bursts and cosmic rays [30], while the Blandford–Znajek mechanism is commonly used to explain active galactic nuclei AGN and quasars, which exhibit powerful jets originating from supermassive black holes located at galaxies' centers. In conclusion, despite their shared characteristics, these processes possess distinct mechanisms and applications.

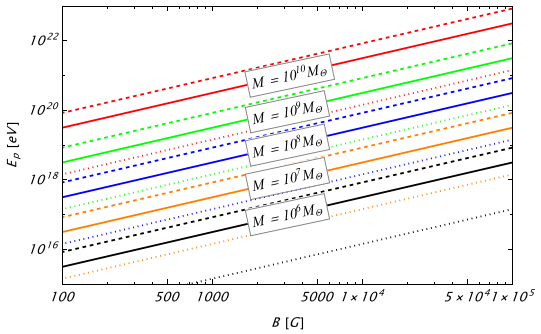

Figure 4. The energy of a proton following neutron beta-decay relies on the magnetic field and different levels of the supermassive black hole's mass. The graph illustrates the outcomes of the Kerr-Taub-NUT black hole and Kerr-MOG black hole using solid and dashed lines, respectively. Conversely, the results for the Kerr black hole are displayed as dotted lines.

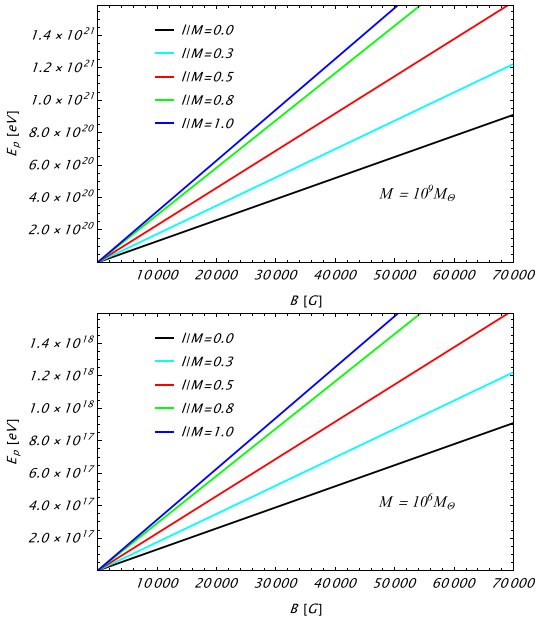

Figure 5. Dependence of the energy of a proton after neutron beta-decay from the magnetic field for different values of dimensionless gravitomagnetic charge.

The MPP finds an intriguing application in elucidating the origins and manufacturing process of ultra-high-energy cosmic rays (UHECR) [49, 50]. The recent pieces of evidence indicate that UHECRs consist of a combination of various particles, whereas earlier measurements indicated a prevalence of proton flow at high energies ([51]). Prominent cosmic ray observatories such as the Pierre Auger Observatory have detected cosmic rays with the highest energy levels originating from beyond our galaxy ([52]). The primary difficulty encountered when investigating ultra-high-energy cosmic rays is their remarkably low occurrence. The frequency of UHECRs possessing an energy surpassing 10^{20} eV is roughly one particle per square kilometer per century. To tackle this challenge, a novel project known as the Cosmic Rays Extremely Distributed Observatory has been suggested, seeking to harness the detection capabilities of countless mobile smartphones worldwide [53]. The possibility of increasing the speed of UHECRs by subjecting them to shock acceleration in the plasma present in relativistic jets exists, but it is uncertain whether this occurs naturally due to the considerable distance required for acceleration and potential losses during interaction within and outside the jet. In contrast, [21] have already utilized a different method called the MPP approach to understanding ultra-high-energy cosmic rays, which does not require a large acceleration region. Instead, their study focuses on the beta-decay of a neutron that is not bound near a supermassive black hole surrounded by an external magnetic field [54]. The MPP can generate protons with energies exceeding 10^{20} eV by exploiting neutron beta-decay in the ergosphere of a supermassive black hole weighing 10^9 times the mass of the Sun and possessing a magnetic field of 10^4 Gauss. We can conclude that the findings from our observations are illustrated in figures 4 and 5, which was generated specifically for the Kerr-Taub-NUT black

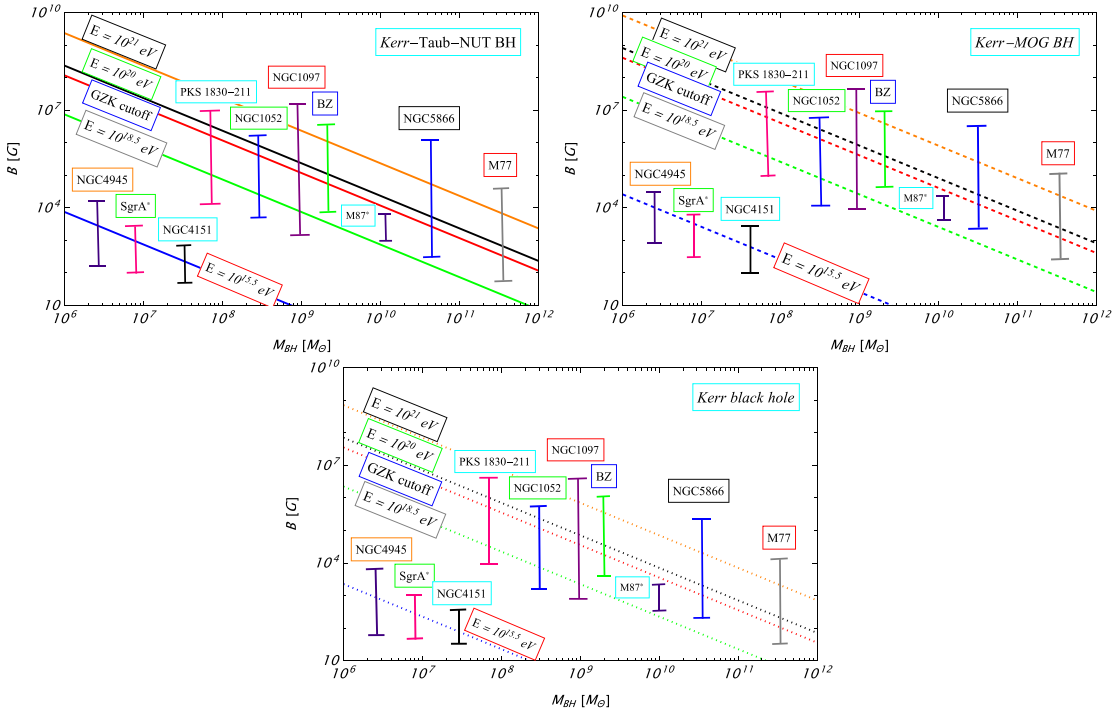

Figure 6. The constraints on the mass and magnetic field of the black hole are responsible for accelerating protons with different energy levels. On the one hand, the solid lines in the upper panel represent the calculated constraints for the Kerr-Taub-NUT black hole, while the dashed lines represent those for the Kerr-MOG black hole. On the other hand, the dotted lines in the center of the bottom panel correspond to the constraints for the Kerr black hole. When comparing the constraints of the Kerr-Taub-NUT black hole to those of Kerr, it becomes evident that the gravitomagnetic charge of the black hole has a significant effect. The energy levels include 10^{20} eV (dashed and solid black), GZK-cutoff $10^{19.7}$eV (dashed and solid red), ankle $10^{18.5}$eV (dashed and solid green), and knee $10^{15.5}$eV (dashed and solid blue). The four vertical bars, each with a different color, indicate potential supermassive black hole candidates such as NGC4945 ([58]), SgrA* ([59]), NGC4151 ([60]), PKS 1830-211 ([61]), NGC1052 ([54]), NGC1097 ([62]), M87* ([63]), NGC5866 ([64]) and M77([65]). The constraints for these candidates have been determined through observation. We opt for the abbreviation BZ to denote the Blandford–Znajek mechanism of relativistic jets, with a supermassive black hole mass of $10^9 M_\odot$ and a magnetic field of $10^4 - 10^7$G. In this scenario, the STVG parameter (α) and the dimensionless gravitomagnetic charge are both set to 0.5.

hole and these results are consistent with recent observations. These primary ultra-high-energy cosmic rays offer valuable insights into the mass, magnetic field, and proximity of the presumed source black hole [55]. Intriguingly, the knee energy of the cosmic ray spectrum around $10^{15.5}$ eV aligns with the maximum energy attainable through the MPP in the supermassive black hole SgrA* located at the center of our galaxy [56, 57]. It is crucial to explore the connections between observed cosmic rays and nearby supermassive black holes that possess predicted mass and magnetic field characteristics according to the MPP.

The acceleration of protons with varying energy levels is influenced by the restrictions imposed on the mass and magnetic field of the black hole. The left panel of figure 6 illustrates the limitations calculated for the Kerr-Taub-NUT black hole, while the right panel depicts those for the Kerr black hole. A comparison of the two reveals that the gravitomagnetic charge of the black hole has a significant impact. The energy levels shown in the figure range from 10^{20}eV (dashed and solid black) to GZK-cutoff ([66]) $10^{19.7}$ eV (dashed and solid red), ankle $10^{18.5}$eV (dashed and solid green), and knee $10^{15.5}$eV (dashed and solid blue). The four vertical bars, each in a different color, represent potential supermassive black hole candidates like NGC4945, SgrA*, NGC4151, PKS1830 − 211, NGC1052, NGC1097, M87*, NGC5866 and M77, whose constraints have been determined through observations ([58, 67–69]). The source identified as BZ aligns with the Blandford–Znajek mechanism of relativistic jets, with a supermassive black hole mass of $10^9 M_\odot$ and a magnetic field of $10^4 - 10^7$G.

4. Conclusions

Our research focuses on energy extraction from black holes based on the circular motion of massive test particles near the Kerr-Taub-NUT and Kerr-MOG black holes, where it has been observed that these particles do not follow a geodesic line due to the presence of a magnetic field. This highlights the impact of magnetic fields on particle motion around black holes. The trajectory of a charged particle is altered by the gravitational field in curved spacetime, resulting in deviations from a standard path.

We have explored the MPP in this context, analyzing the efficiency of energy extraction by applying conservation laws to particle parameters before and after decay near a black hole. Relativistic charged particles like electrons and protons experience synchrotron radiation loss in the presence of a magnetic field, leading to significant changes in their energy and angular momentum. This allows for a comparison with other energy extraction models, including the Blandford–Znajek mechanism. To begin with, our initial focus was to analyze the MPP classification based on varying levels of energy efficiency. Through our study, we demonstrated that these three categories of magnetic Penrose processes yield noteworthy outcomes that are comparable to observational findings. We can offer insights to evaluate the entire process of our work:

(a) In figure 2, it can be seen that in the absence of a magnetic field, the Kerr-Taub-NUT black hole can achieve a maximum energy extraction efficiency of about $\sim 36\%$ for a specific value of the dimensionless gravitomagnetic charge. On the other hand, if the black hole does not have a gravitomagnetic charge, we can go back to the original Penrose process, where the efficiency η_{PP} is approximately 0.207, corresponding to around 20.7%. This efficiency value is for an extremely rotating Kerr black hole.

(b) When a magnetic field is present, the moderate regime of the magnetic Penrose process occurs when the charge q_3 is greater than q_1, effectively opposing the gravitational electric field generated by a black hole. This requires certain conditions, namely, when magnetic fields are present for elementary particles, the electromagnetic forces become dominant within the system, indicating that the product of the charge-to-mass ratio $(\frac{q}{m})$ and the component of the magnetic vector potential (A_t) is much larger than the product of the particle's mass (m) and the component of the four-velocity vector in the time direction (u_t).

(c) It is important to note that equation (36) is crucial in understanding the behavior of the MPP in the ultra-high efficiency regime. This equation provides insight into the transfer of energy to the escaping particle and allows us to assess the effectiveness of the process. Figure 3 provides a visual representation of the assessment of the MPP's efficiency in the ultra-high regime for different types of black holes. The two categories of black holes considered are a stellar mass black hole, which weighs about 10 times that of the Sun, and a supermassive black hole, which weighs approximately 10^9 times that of the Sun. Based on our observations, it can be inferred that the data presented in figure 6 pertains to the Kerr-Taub-NUT black hole versus to Kerr-MOG black hole and the results obtained from our analysis align with the observations made. They demonstrate that the gravitomagnetic charge and MOG parameter can amplify the MPP in achieving a state of ultra-high efficiency ([70]). This assessment of the MPP's effectiveness in the ultra-high regime in the presence of the gravitomagnetic charge and MOG parameter provides valuable insights into the behavior of black holes and their interaction with surrounding particles. It deepens our understanding of the mechanisms at play in these extreme astrophysical systems.

(d) The mass and magnetic field constraints of the black hole are responsible for accelerating protons at various energy levels. However, it is important to note that, in figure 6, the left and right sides of the upper panel specifically display calculated constraints for the Kerr-Taub-NUT black hole and Kerr-MOG black hole, while the results in the center of the bottom panel pertain to the Kerr black hole. Comparing the constraints of these two types of black holes reveals the significant influence of the gravitomagnetic charge. The energy levels considered in the analysis include 10^{20}eV (represented by dashed and solid black lines), GZK-cutoff ([71]) $10^{19.7}$eV (represented by dashed and solid red lines), ankle $10^{18.5}$eV (represented by dashed and solid green lines), and knee $10^{15.5}$eV (represented by dashed and solid blue lines). Four colored vertical bars indicate potential supermassive black hole candidates such as NGC4945, PKS1830 − 211, SgrA*, NGC4151, NGC1052, NGC1097, M87*, NGC5866 and M77 ([54, 60, 63, 67, 72, 73]), with their respective constraints determined through observations. Additionally, the source referred to as BZ aligns with the Blandford–Znajek mechanism of relativistic jets, characterized by a supermassive black hole mass of $10^9 M_\odot$ and a magnetic field ranging from 10^4 to 10^7G

The MPP has primarily been examined in connection with phenomena such as gamma-ray bursts and cosmic rays, while the Blandford–Znajek mechanism is frequently employed to elucidate AGN and quasars. These objects demonstrate formidable jets originating from supermassive black holes situated at the centers of galaxies ([51]). In the presence of gravitomagnetic charge and MOG parameter, the MPP is capable of producing protons with energy levels surpassing 10^{20}eV by utilizing the ergosphere of an enormous supermassive black hole, which is 1 billion times heavier than the Sun and possesses a magnetic field strength of 10^4 Gauss. This process makes use of neutron beta decay. Figure 4 illustrates this phenomenon and it serves as a crucial method for obtaining insights into the mass, magnetic field, gravitomagnetic charge, and proximity of the assumed source black hole. Additionally, this offers valuable information concerning the

primary ultra-high-energy cosmic rays. Examining the links between observed cosmic rays and neighbouring supermassive black holes, as per the MPP, holds significant importance. In addition, the Kerr-MOG spacetime exhibits higher energy extraction efficiency compared to the Kerr-Taub-NUT spacetime. This conclusion is supported by the evidence presented in figure 6, which demonstrates that the magnetic field strength surrounding the Kerr-MOG black hole is stronger in comparison to that surrounding Kerr-Taub-NUT and Kerr black holes. This graph serves as the main basis for drawing this conclusion, and additionally, the paper strives to provide further support for this relationship across potential supermassive black hole candidates.

Data availability statement

The data cannot be made publicly available upon publication because they contain sensitive personal information. The data that support the findings of this study are available upon reasonable request from the authors.

Acknowledgments

This research was supported by the Grants F-FA-2021-510 from the Uzbekistan Ministry for Innovative Development.

Appendix A. Kerr-MOG black hole

In the Boyer–Lindquist coordinates, the exterior spacetime of the Kerr-MOG black hole is described by the line element [18]:

$$ds^2 = -\frac{\Delta}{\Sigma}\left(dt - a\sin^2\theta d\phi\right)^2 + \Sigma d\theta^2 + \frac{\Sigma}{\Delta}dr^2 + \frac{\sin^2\theta}{\Sigma}\left[\left(r^2+a^2\right)d\phi - adt\right]^2 , \tag{A.1}$$

where

$$\begin{aligned}\Delta &= r^2 - 2(1+\alpha)Mr + \alpha(1+\alpha)M^2 + a^2 ,\\ \Sigma &= r^2 + a^2\cos^2\theta ,\end{aligned} \tag{A.2}$$

M and a represent the total mass and spin of the black hole, respectively, while α denotes the parameter of the STVG theory [10].

In the preceding research, we analyzed the motion of massive charged particles around a black hole in the STVG theory [31]. In contrast to other theories of gravity [18], these particles do not follow the geodesic line. Hence, in the presence of the magnetic field, their equation of motion is governed by the equation stated in [74]:

$$\ddot{x}^\mu + \Gamma^\mu_{\nu\lambda}\dot{x}^\nu\dot{x}^\lambda = \frac{q_g}{m}B^\mu_{\ \nu}\dot{x}^\nu + \frac{q}{m}F^\mu_{\ \nu}\dot{x}^\nu , \qquad \dot{x}^\mu = \frac{dx^\mu}{ds} , \tag{A.3}$$

the Lagrangian can be presented as the following expression

$$\mathcal{L} = \frac{1}{2}g_{\mu\nu}\dot{x}^\mu\dot{x}^\nu + \frac{q_g}{m}\Phi_\mu\dot{x}^\mu + \frac{q}{m}A_\mu\dot{x}^\mu , \tag{A.4}$$

where the particle's mass is represented by m and its gravitational charge is expressed as $q_g = \sqrt{\alpha G_N}m$, where α is a dimensionless scalar field, also known as coupling constant of the interaction between the particle and the fifth force in STVG theory, G_N is Newton's gravitational constant, and q is charge of the particle moving in electromagnetic field. It is important to note that the vector potential Φ_α for the spacetime (A.1) plays a significant role in representing the fifth interaction between a test body and an external vector field. In static spacetime, this interaction is characterized by a Coulomb-like potential. However, in the spacetime of rotating gravitational objects, further advancements can be made in the vector potential

$$\Phi_\mu = \frac{\sqrt{\alpha}Mr}{\Sigma}\left(-1,0,0,a\sin^2\theta\right) . \tag{A.5}$$

The equation governing the Hamilton–Jacobi formalism for a particle with mass m can be represented in the form given by [44].

$$g^{\mu\nu}\left(\frac{\partial \mathcal{S}}{\partial x^{\mu}}-q_g\Phi_{\mu}-qA_{\mu}\right)\left(\frac{\partial \mathcal{S}}{\partial x^{\nu}}-q_g\Phi_{\nu}-qA_{\nu}\right)=-m^2\,. \tag{A.6}$$

As the above method in section 2, by considering the specific conditions of a massive particle in a circular orbit with both zero radial velocity and zero angular velocity, it becomes evident that the particle's motion is limited within a specific range. This can be better comprehended by analyzing the effective potential, as discussed in previous works such as [23, 31, 45]

$$V_{eff}=-\frac{q}{m}A_t-\frac{q_g}{m}\Phi_t+\omega\left(\mathcal{L}-\frac{q}{m}A_{\phi}-\frac{q_g}{m}\Phi_{\phi}\right)+\left[(-\psi)\left(\frac{\left(\mathcal{L}-\frac{q}{m}A_{\phi}-\frac{q_g}{m}\Phi_{\phi}\right)^2}{g_{\phi\phi}}+1\right)\right]^{\frac{1}{2}}\,. \tag{A.7}$$

The effective potential is a widely recognized method for understanding the behavior of test particles near black holes and meeting the requirement of $E=V_{\rm eff}$ allows for its implementation. By identifying the minimum value of the effective potential, we can determine the ISCO, which represents the shortest path where a particle can maintain a stable circular trajectory without being pulled into the black hole or thrown into space. To simplify the analysis, we focus on the equatorial plane, and the effective potential becomes solely dependent on the radial coordinate, denoted as $V_{\rm eff}(r)$. The ISCO can be determined using the conventional method by ensuring that the effective potential is equal to the particle's energy ($V_{\rm eff}(r)=E$), the derivative of the effective potential with respect to r is zero ($V'_{\rm eff}(r)=0$), and the second derivative of the effective potential with respect to r is less than or equal to zero ($V''_{\rm eff}(r)\leqslant 0$). However, it should be noted that computing the equation (A.7) analytically is extremely challenging. Nevertheless, emphasizing the significance of the ISCO in astrophysical observations is crucial, as it greatly affects radiation release and the behavior of matter near the black hole. Furthermore, studying the ISCO can provide valuable knowledge about the properties of black holes and can serve as a platform to investigate general relativity and alternative theories of gravity.

Appendix B. Parameters C_1 and C_2

Electromagnetic field's vector potential A_{α}, under the Lorentz gauge, in a simplified form [41]

$$A^{\mu}=C_1\xi^{\mu}_{(t)}+C_2\xi^{\mu}_{(\phi)}\,. \tag{B.1}$$

here, we have the constant C_2 denoted as $B/2$, which represents a uniform magnetic field B parallel to the axis of rotation, surrounding the gravitational source. Determining the value of the remaining constant C_1 is a straightforward task accomplished by examining the asymptotic properties of spacetime as it extends toward infinity. To establish the value of the remaining constant, one can rely on the electrical neutrality of the source [39, 75]

$$\frac{1}{2}\oint F^{\mu\nu}_{*}dS_{\mu\nu}=C_1\oint\Gamma^{\mu}_{\mu\sigma}u_{\mu}m^{\nu}\xi^{\sigma}_{(t)}\,(uk)\,dS+\frac{B}{2}\oint\Gamma^{\mu}_{\mu\sigma}u_{\mu}m^{\nu}\xi^{\sigma}_{(\phi)}\,(uk)\,dS=0\,. \tag{B.2}$$

By performing the integration over the spherical surface at asymptotic infinity, the value can be obtained. In this calculation, we employ the equality $\xi\nu;\mu=-\xi\mu;\nu=-\Gamma^{\sigma}_{\mu\nu}\xi_{\sigma}$, which arises from the Killing equation. Additionally, the element of an arbitrary 2-surface, $dS^{\mu\nu}$, is expressed in a specific form [76]

$$dS^{\mu\nu}=-u^{\mu}\wedge m^{\nu}\,(uk)\,dS+\eta^{\mu\nu\alpha\beta}u_{\mu}u_{\nu}\sqrt{1+(uk)^2}dS\,, \tag{B.3}$$

where

$$m_{\mu}=\frac{\eta_{\lambda\mu\alpha\beta}u^{\lambda}n^{\alpha}k^{\beta}}{\sqrt{1+(uk)^2}}\,,\quad n_{\mu}=\frac{\eta_{\lambda\mu\alpha\beta}u^{\lambda}k^{\alpha}m^{\beta}}{\sqrt{1+(uk)^2}}\,,$$
$$k^{\mu}=-\,(uk)\,u^{\mu}+\sqrt{1+(uk)^2}\eta^{\alpha\mu\gamma\beta}u_{\alpha}m_{\gamma}n_{\beta} \tag{B.4}$$

where, the triple of vectors k, m, n exhibit the following relationships: n^{μ} denotes the vector normal to the 2-surface, n^{ν} represents a space-like vector within the given 2-surface that is orthogonal to the four-velocity of the observer u^{ν}, and k^{ν} is a unit space-like four-vector that belongs to the surface and is orthogonal to m^{ν}. The symbol dS corresponds to the invariant element of the surface, $\wedge$ denotes the wedge product, $_*$ is used

for the dual element, and $\eta_{\mu\nu\sigma\delta}$ represents the pseudo-tensorial expression for the Levi-Civita symbol $\epsilon_{\mu\nu\sigma\delta}$. By substituting $u_0 = -(1 - M/r)$, $m^1 = (1 - M/r)$, and the asymptotic values for the Christoffel symbols $\Gamma^0_{10} = M/r^2$ and $\Gamma^0_{13} = -3aM\sin^2\theta/r^2 - l(1 - 2M/r)\cos\theta/r$ into the flux expression (6), we can determine the value of the constant $C_1 = aB$. The parameter l does not affect the constant C_1 because the integral $\int_0^\pi \cos\theta \sin\theta \, d\theta = 0$ results in its vanishing.

ORCID iD

Husan Alibekov https://orcid.org/0009-0007-9968-7066

References

[1] Akiyama K *et al* (Event Horizon Telescope Collaboration) 2019 First M87 event horizon telescope results. I. The shadow of the supermassive black hole *Astrophys. J. Lett.* **875** L1
[2] Bambi C, Freese K, Vagnozzi S and Visinelli L 2019 Testing the rotational nature of the supermassive object M87* from the circularity and size of its first image *Phys. Rev.* D **100** 044057
[3] Newman E, Tamburino L and Unti T 1963 Empty space generalization of the Schwarzschild metric *J. Math. Phys.* **4** 915
[4] Ghasemi-Nodehi M, Chakraborty C, Yu Q and Lu Y 2021 Investigating the existence of gravitomagnetic monopole in M87* *Eur. Phys. J.* C **81** 939
[5] Chakraborty C and Bhattacharyya S 2022 Primordial black holes having gravitomagnetic monopole *Phys. Rev.* D **106** 103028
[6] Chakraborty C and Bhattacharyya S 2019 Circular orbits in Kerr-Taub-NUT spacetime and their implications for accreting black holes and naked singularities *J. Cosmol. Astropart. Phys.* JCAP05(2019)034
[7] Virmani A 2011 Asymptotic flatness, Taub-NUT and variational principle *Phys. Rev.* D **84** 064034
[8] Kagramanova V, Kunz J, Hackmann E and Lämmerzahl C 2010 Analytic treatment of complete and incomplete geodesics in Taub-NUT space-times *Phys. Rev.* D **81** 124044
[9] Ramaswamy S and Sen A 1986 Comment on "gravitomagnetic pole and mass quantization" *Phys. Rev. Lett.* **57** 1088
[10] Moffat J W 2006 Scalar-tensor-vector gravity theory *J. Cosmol. Astropart. Phys.* JCAP03(2006)004
[11] Moffat J W and Rahvar S 2013 The MOG weak field approximation and observational test of galaxy rotation curves *Mon. Not. Roy. Astron. Soc.* **436** 1439–51
[12] Moffat J W and Toth V T 2015 Rotational velocity curves in the Milky Way as a test of modified gravity *Phys. Rev.* D **91** 043004
[13] Moffat J W 2015 Modified gravity black holes and their observable shadows *Eur. Phys. J.* C **75** 130
[14] Sau S and Moffat J W 2023 Shadow of a regular black hole in scalar-tensor-vector gravity theory *Phys. Rev.* D **107** 124003
[15] Moffat J W 2006 Gravitational lensing in modified gravity and the lensing of merging clusters without dark matter (arXiv:astro-ph/0608675)
[16] Moffat J W and Toth V T 2009 The bending of light and lensing in modified gravity *Mon. Not. R. Astron. Soc.* **397** 1885–992
[17] Moffat J W 2014 Scalar and vector field constraints, deflection of light and lensing in modified gravity (MOG) (arXiv:1410.2464[gr-qc])
[18] Moffat J W 2015 Black holes in modified gravity (MOG) *Eur. Phys. J.* C **75** 175
[19] Moffat J W 2021 Modified gravity (MOG), cosmology and black holes *J. Cosmol. Astropart. Phys.* JCAP02(2021)017
[20] Moffat J W, Rahvar S and Toth V T 2018 Applying MOG to lensing: Einstein rings, Abell 520 and the bullet cluster *Galaxies* **6** 43
[21] Tursunov A and Dadhich N 2019 Fifty years of energy extraction from rotating black hole: revisiting magnetic penrose process *Universe* **5** 125
[22] Shaymatov S, Ahmedov B, Stuchlík Z and Abdujabbarov A 2018 Effect of an external magnetic field on particle acceleration by a rotating black hole surrounded with quintessential energy *Int. J. Mod. Phys.* D **27** 1850088
[23] Stuchlík Z, Kološ M and Tursunov A 2021 Penrose process: its variants and astrophysical applications *Universe* **7** 416
[24] Penrose R and Floyd R M 1971 Extraction of rotational energy from a black hole *Nat. Phys. Sci.* **229** 177–9
[25] Abdujabbarov A A, Ahmedov B J, Shaymatov S R and Rakhmatov A S 2011 Penrose process in Kerr-Taub-NUT spacetime *Astrophys. Space Sci.* **334** 237–41
[26] Blandford R D and Znajek R L 1977 Electromagnetic extraction of energy from Kerr black holes *Mon. Not. R. Astron. Soc.* **179** 433–56
[27] Wagh S M, Dhurandhar S V and Dadhich N 1985 Revival of the Penrose process for astrophysical applications *Astrophys. J.* **290** 12
[28] Shaymatov and S, Vrba J, Malafarina D, Ahmedov B and Stuchlík Z 2020 Charged particle and epicyclic motions around 4D Einstein-Gauss-Bonnet black hole immersed in an external magnetic field *Phys. Dark Universe* **30** 100648
[29] Dadhich N 2012 Magnetic penrose process and Blanford-Zanejk mechanism: a clarification (arXiv:1210.1041)
[30] Dadhich N , Tursunov A, Ahmedov B and Stuchlík Z 2018 The distinguishing signature of magnetic Penrose process *Mon. Not. R. Astron. Soc.* **478** L89–L94
[31] Turimov B, Alibekov H, Tadjimuratov P and Abdujabbarov A 2023 Gravitational synchrotron radiation and penrose process in STVG theory *Phys. Lett.* B **843** 138040
[32] Dadhich N and Turakulov Z Y 2002 The most general axially symmetric electrovac spacetime admitting separable equations of motion *Class. Quantum Grav.* **19** 2765
[33] Bunster C W, Portugues R, Cnockaert S and Henneaux M 2006 Monopoles for gravitation and for higher spin fields *Phys. Rev.* D **73** 105014
[34] Regge T and Teitelboim C 1974 Role of surface integrals in the hamiltonian formulation of general relativity *Ann. Phys., NY* **88** 286–318
[35] Narzilloev B , Abdujabbarov A, Ahmedov B and Bambi C 2023 Kerr-Taub-NUT spacetime to explain the jet power and the radiative efficiency of astrophysical black holes *Phys. Rev.* D **108** 103013
[36] Carroll S M 2019 *Spacetime and Geometry: An Introduction to General Relativity* (Cambridge University Press)
[37] Hawking S W and Ellis G F R 2023 *The Large Scale Structure of Space-Time* (*Cambridge Monographs on Mathematical Physics*) (Cambridge University Press)
[38] Wald R M 1974 Black hole in a uniform magnetic field *Phys. Rev.* D **10** 1680–5

[39] Abdujabbarov A A , Ahmedov B J and Kagramanova V G 2008 Particle motion and electromagnetic fields of rotating compact gravitating objects with gravitomagnetic charge *Gen. Relativ. Gravit.* **40** 2515–32
[40] Aliev A N 2006 A slowly rotating charged black hole in five dimensions *Mod. Phys. Lett.* A **21** 751–8
[41] Tursunov A, Stuchlík Z and Kološ M 2016 Circular orbits and related quasiharmonic oscillatory motion of charged particles around weakly magnetized rotating black holes *Phys. Rev.* D **93** 084012
[42] Stuchlík Z and Kološ M 2016 Acceleration of the charged particles due to chaotic scattering in the combined black hole gravitational field and asymptotically uniform magnetic field *Eur. Phys. J.* C **76** 32
[43] Aliev A N and Frolov V P 2004 Five-dimensional rotating black hole in a uniform magnetic field: the gyromagnetic ratio *Phys. Rev.* D **69** 084022
[44] Chandrasekhar S 1984 *The Mathematical Theory of Black Holes* vol 9 (Springer) (https://doi.org/10.1007/978-94-009-6469-3_2)
[45] Bhat M, Dhurandhar S and Dadhich N 1985 Energetics of the Kerr-Newman black hole by the Penrose process *J. Astrophys. Astron.* **6** 85–100
[46] Parthasarathy S, Wagh S M, Dhurandhar S V and Dadhich N 1986 High efficiency of the penrose process of energy extraction from rotating black holes immersed in electromagnetic fields *Astrophys. J.* **307** 38
[47] Romero G and Vila G 2013 *Introduction to Black Hole Astrophysics* 1 edn vol 876 (Springer) (https://doi.org/10.1007/978-3-642-39596-3)
[48] Bambi C 2017 *Black Holes: A Laboratory for Testing Strong Gravity* 1 edn (Springer) (https://doi.org/10.1007/978-981-10-4524-0)
[49] Coleman A *et al* 2023 Ultra high energy cosmic rays the intersection of the cosmic and energy frontiers *Astropart. Phys.* **149** 102819
[50] Tursunov A *et al* 2021 Acceleration of ultra-high-energy cosmic rays by local supermassive black hole candidates *PoS* **ICRC2021** 471
[51] Zajaček M *et al* 2018 On the charge of the galactic centre black hole *Mon. Not. R. Astron. Soc.* **480** 4408–23
[52] Aab A *et al* 2017 Pierre Auger collaboration "observation of a large-scale anisotropy in the arrival directions of cosmic rays above 8×10^{18} eV" *Science* **357** 1266–70
[53] Góra D 2018 Cosmic-ray extremely distributed observatory: status and perspectives *Universe* **4** 111
[54] Parsa M, Eckart A, Shahzamanian B, Karas V, Zajaček M, Zensus J A and Straubmeier C 2017 Investigating the relativistic motion of the stars near the supermassive black hole in the galactic center *Astrophys. J.* **845** 22
[55] Abbasi RU *et al* 2017 Search for EeV protons of galactic origin *Astropart. Phys.* **86** 21–26
[56] Eatough R P *et al* 2013 A strong magnetic field around the supermassive black hole at the centre of the galaxy *Nature* **501** 391–4
[57] Morris M R 2015 Manifestations of the galactic center magnetic field *Lessons from the Local Group: A Conference in Honour of David Block and Bruce Elmegreen* p 391
[58] Wojaczyński R and Niedźwiecki A 2017 The X-/γ-ray correlation in NGC 4945 and the nature of its γ-ray source *Astrophys. J.* **849** 97
[59] Stein W A and Forrest W J 1986 Infrared point sources aligned with the SgrA* non-thermal radio source *Nature* **323** 232–4
[60] Peretti E *et al* 2023 Gamma-ray emission from the Seyfert galaxy NGC 4151 and multimessenger implications for ultra-fast outflows (arXiv:2303.03298 [astro-ph.HE])
[61] Zhang S, Chen Y-P, Collmar W, Foschini L, Li T-P, Torres D F and Wang J-M 2008 High-energy properties of PKS 1830-211 *Astrophys. J.* **683** 400–8
[62] Quillen A C, Frogel J A, Kuchinski L E and Terndrup D M 1995 Multiband images of the barred galaxy NGC 1097 *Astrophys. J.* **110** 156
[63] Dainotti M G, Ostrowski M, Harris D, Siemiginowska A and Siejkowski H 2012 A cosmic ray cocoon along the x-ray jet of M87? *Mon. Not. R. Astron. Soc.* **426** 218–25
[64] Li J-T, Wang Q D, Li Z and Chen Y 2009 Dynamic S0 galaxies: a case study of NGC 5866 *Astrophys. J.* **706** 693
[65] Tagawa H *et al* 2023 High-energy electromagnetic, neutrino, and cosmic-ray emission by stellar-mass black holes in disks of active galactic nuclei (arXiv:2307.06353)
[66] Zatsepin G T and Kuz'min V A 1966 Upper limit of the spectrum of cosmic rays *Sov. J. Exp. Theor. Phys. Lett.* **4** 78
[67] IceCube Collaboration 2021 Detection of a particle shower at the Glashow resonance with IceCube *Nature* **591** 220–4
[68] Eckart A *et al* 2012 Millimeter to x-ray flares from sagittarius A* *Astron. Astrophys.* **537** A52
[69] Baczko A-K *et al* 2016 A highly magnetized twin-jet base pinpoints a supermassive black hole *Astron. Astrophys.* **593** A47
[70] Tursunov A, Stuchlík Z, Kološ M, Dadhich N and Ahmedov B 2020 Supermassive black holes as possible sources of ultrahigh-energy cosmic rays *Astrophys. J.* **895** 14
[71] Greisen K 1966 End to the cosmic-ray spectrum? *Phys. Rev. Lett.* **16** 748–50
[72] Kino M, Takahara F, Hada K, Akiyama K, Nagai H and Sohn B W 2015 Magnetization degree at the jet base of M87 derived from the event horizon telescope data: testing the magnetically driven jet paradigm *Astrophys. J.* **803** 30
[73] Zajaček M *et al* 2019 Constraining the charge of the galactic centre black hole *J. Phys.: Conf. Ser.* **1258** 012031
[74] Moffat J W 2011 Modified gravity or dark matter? (arXiv:1101.1935v2 [astro-ph.CO])
[75] Bičák J and Janiš V 1985 Magnetic fluxes across black holes *Mon. Not. R. Astron. Soc.* **212** 899–915
[76] Ahmedov B J and Rakhmatov N I 2003 Concerning measurement of gravitomagnetism in electromagnetic systems *Found. Phys.* **33** 625–39